

# Non-additivity of van der Waals forces on liquid surfaces

Prashanth S. Venkataram,<sup>1</sup> Jeremy D. Whitton,<sup>2</sup> and Alejandro W. Rodriguez<sup>1</sup>

<sup>1</sup>*Princeton University, Department of Electrical Engineering, Princeton, New Jersey 08544, USA*

<sup>2</sup>*Princeton University, Department of Physics, Princeton, New Jersey 08544, USA*

(Dated: April 20, 2016)

We present an approach for modeling nanoscale wetting and dewetting of liquid surfaces that exploits recently developed, sophisticated techniques for computing van der Waals (vdW) or (more generally) Casimir forces in arbitrary geometries. We solve the variational formulation of the Young–Laplace equation to predict the equilibrium shapes of fluid–vacuum interfaces near solid gratings and show that the non-additivity of vdW interactions can have a significant impact on the shape and wetting properties of the liquid surface, leading to very different surface profiles and wetting transitions compared to predictions based on commonly employed additive approximations, such as Hamaker or Derjaguin approximations.

Wetting and dewetting phenomena are ubiquitous in soft matter systems and have a profound impact on many disciplines, including biology [1], microfluidics [2], and microfabrication [3]. One problem of great interest concerns the suspension of fluid films on or near structured surfaces where, depending on the interplay of competing short-range molecular or capillary forces (e.g. surface tension), gravity, and long-range dispersive interactions (i.e. van der Waals or more generally, Casimir forces), the film may undergo wetting or dewetting transitions, or exist in some intermediate state, forming a continuous surface profile of finite thickness [2, 4]. Thus far, theoretical analyses of these competing effects have relied on approximate descriptions of the dispersive van der Waals (vdW) forces [5–7], i.e. so-called Derjaguin [8] and Hamaker [9] approximations, which have recently been shown to fail when applied in regimes that fall outside of their narrow range of validity [5, 10–12].

In this paper, building on recently developed theoretical techniques for computing Casimir forces in arbitrary geometries [13, 14], we demonstrate an approach for studying the equilibrium shapes (the wetting and dewetting properties) of liquid surfaces that captures the full non-additivity and non-locality of vdW interactions [15]. As a proof of concept, we consider the problem of a fluid surface on or near a periodic grating, idealized as a deformable perfect electrical conductor (PEC) surface (playing the role of a fluid surface) interacting through vacuum below a fixed periodic PEC grating [Fig. 1], and show that the competition between surface tension and non-additive vdW pressure leads to quantitatively and qualitatively different equilibrium fluid shapes and wetting properties compared with predictions based on commonly employed additive approximations. Our simplifying choice of PEC surfaces allows for a scale-invariant analysis of the role of geometry on both non-additivity and fluid deformations, ignoring effects associated with material dispersion that would otherwise further complicate our analysis and which are likely to result in even larger deviations [5, 16]. Our results provide a basis for experimental studies of fluid suspensions in situations where vdW non-additivity can have a significant impact.

Equilibrium fluid problems are typically studied by way of

the augmented Young-Laplace equation [17],

$$\gamma \nabla \cdot \left( \frac{\nabla \Psi}{\sqrt{1 + |\nabla \Psi|^2}} \right) + \frac{\delta}{\delta \Psi} (\mathcal{E}_{\text{other}}[\Psi] + \mathcal{E}_{\text{vdW}}[\Psi]) = 0 \quad (1)$$

describing the local balance of forces (variational derivatives of energies) acting on a fluid of surface profile  $\Psi(\mathbf{x})$ . The first two terms describe surface and other external forces (e.g. gravity), with  $\gamma$  denoting the fluid–vacuum surface tension, while the third term  $\frac{\delta}{\delta \Psi} \mathcal{E}_{\text{vdW}}$  denotes the local disjoining pressure arising from the changing vdW fluid–substrate interaction energy  $\mathcal{E}_{\text{vdW}}$ . Semi-analytical [18, 19] and brute-force [20, 21] solutions of the YLE have been pursued in order to examine various classes of wetting problems, including those arising in atomic force microscopy, wherein a solid object (e.g. spherical tip) is brought into close proximity to a fluid surface [18–20], or those involving liquids on chemically [22, 23] or physically [2, 4, 21] textured surfaces.

A commonality among prior theoretical studies of (1) is the use of simple, albeit heuristic approximations that treat vdW interactions as additive forces, often depending on the shape of the fluid in a power-law fashion [8, 9, 24]. Derjaguin or proximity-force approximations (PFA) are applicable in situations involving nearly planar structures, i.e. small curvatures compared to their separation, approximating the interaction between the objects as an additive, pointwise summation of plate–plate interactions between differential elements comprising their surfaces [8, 24]. Hamaker or pairwise-summation (PWS) approximations are applicable in situations involving dilute media [11], approximating the interaction between two objects as arising from the pairwise summation of (dipolar) London–vdW [25] or Casimir–Polder [26] forces between volumetric elements of the same constitutive materials [9]; such a treatment necessarily neglects multiple-scattering and other non-additive effects. When applied to geometries consisting of planar interfaces, PFA can replicate exact results based on the so-called Lifshitz theory (upon which it is based) [27], whereas PWS captures the distance dependence obtained by exact calculations but differs in magnitude (except in dilute situations) [11]. Typically, the quantitative discrepancy of PWS is rectified via a renormalization of the force coefficient to that of the Lifshitz formula, widely known

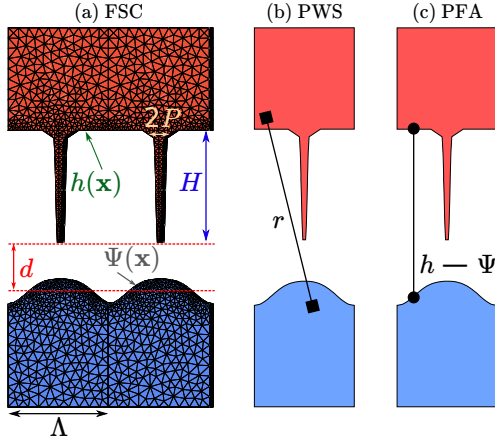


Figure 1. Schematic of fluid-grating geometry comprising a fluid (blue) of surface profile  $\Psi(\mathbf{x})$  in close proximity (average distance  $d$ ) to a solid grating (red) of height profile  $h(\mathbf{x})$ , involving thin nanorods of height  $H$ , thickness  $2P$ , and period  $\Lambda$ . (a) Representative mesh employed by a recently developed FSC boundary-element method [33] for computing exact vdW energies in complex geometries. (b) and (c) illustrate commonly employed pairwise-summation (PWS) and proximity-force approximations (PFA), involving volumetric and surface interactions throughout the bodies, respectively.

as the Hamaker constant [28].

The inadequacy of these additive approximations in situations that fall outside of their range of validity has been a topic of significant interest, spurred by the recent development of techniques that take full account of complicated non-additive and boundary effects arising in non-planar structures, revealing non-monotonic, logarithmic, and even repulsive interactions stemming from geometry alone [5, 15, 29, 30]. These brute-force techniques share little semblance with additive approximations, which offer computational simplicity and intuition at the expense of neglecting important electromagnetic effects. In particular, the exact vdW energy in these modern formulations is often cast as a log-determinant expression involving the full (no approximations) electromagnetic scattering properties of the individual objects, obtained semi-analytically or numerically by exploiting spectral or localized basis expansions of the scattering unknowns [5, 31]. The generality of these methods does, however, come at a price, with even the most sophisticated of formulations requiring thousands or hundreds of thousands of scattering calculations to be performed [5]. Despite the fact that fluid suspensions motivated much of the original theoretical work on vdW interactions between macroscopic bodies [6, 7, 27, 32], to our knowledge these recent techniques have yet to be applied to wetting problems in which non-additivity and boundary effects are bound to play a significant role on fluid deformations.

*Methods.*— In order to solve (1) in general settings, we require knowledge of  $\frac{\delta}{\delta\Psi} \mathcal{E}_{\text{vdW}}[\Psi]$  for arbitrary  $\Psi$ . We employ a mature and freely available method for computing vdW interactions in arbitrary geometries and materials [33, 34], based on the fluctuating-surface current (FSC) framework [13, 14]

of electromagnetic scattering, in which the vdW energy,

$$\mathcal{E}_{\text{FSC}} = \frac{\hbar}{2\pi} \int_0^\infty d\xi \ln(\det(\mathbb{M}\mathbb{M}_\infty^{-1})) \quad (2)$$

is expressed in terms of “scattering” matrices  $\mathbb{M}$ ,  $\mathbb{M}_\infty$  involving interactions of surface currents (unknowns) flowing on the boundaries of the bodies [13, 14] and integrated along imaginary frequencies  $\xi = i\omega$ ; these are computed numerically via expansions in terms of localized basis functions, or triangular meshes interpolated by linear polynomials [Fig. 1(a)], in which case it is known as a boundary element method. Because exact methods most commonly yield the total vdW energy or force, rather than the local pressure on  $\Psi$ , it is convenient to consider the YLE in terms of an equivalent variational problem for the total energy [35, 36]:

$$\min_{\Psi} \left( \gamma \int \sqrt{1 + |\nabla\Psi|^2} + \mathcal{E}_{\text{other}}[\Psi] + \mathcal{E}_{\text{vdW}}[\Psi] \right), \quad (3)$$

where just as in (1), the first term captures the surface energy, the second captures contributions from gravity or bulk thermodynamic/fluid interactions, and the third captures the dispersive vdW interaction energy. For simplicity, we ignore other competing interactions, including thermodynamic and viscous forces [19, 20] and neglect gravity when considering nanoscale fluid deformations, focusing instead only on the impact of surface and dispersive vdW interactions.

Equation 3 can be solved numerically via any number of available nonlinear optimization/minimization techniques [35, 36], requiring only a convenient parametrization of  $\Psi$  using a finite number of degrees of freedom. In what follows, we consider numerical solution of (3) for the particular case of a deformable incompressible PEC surface  $\Psi$  interacting through vacuum with a 1d-periodic PEC grating of period  $\Lambda$  and shape  $h(\mathbf{x}) = d - H \left( \frac{1}{e^{\alpha(x-P)} + 1} + \frac{1}{e^{-\alpha(x+P)} + 1} - 2 \right)$ , for  $|x| < \frac{\Lambda}{2}$ , with half-pitch  $P = 0.03\Lambda$  and height  $H = 1.2\Lambda$ . Figure 1 shows the grating surface and fluid profile obtained by solving (3) for a representative set of parameters and mesh discretization. Here,  $d = 0.4\Lambda$  is the initial minimum grating-fluid separation, and  $\alpha\Lambda = 150$  is a parameter that smoothens otherwise sharp corners in the grating, alleviating spatial discretization errors in the calculation of  $\mathcal{E}_{\text{vdW}}$  while having a negligible impact on the qualitative behavior of the energy compared to what one might expect from more typical, piecewise-constant gratings [10].

To minimize the energy, we employ a combination of algorithms found in the NLOPT optimization suite [37–39]. Although the localized basis functions or mesh of the FSC method provide one possible parametrization of the surface, for the class of periodic problems explored here, a simple Fourier expansion of the surface provides a far more efficient and convenient basis, requiring far fewer degrees of freedom to describe a wide range of periodic shapes. Because the grating is translationally invariant along the  $z$  direction and mirror-symmetric about  $x = 0$ , we parametrize  $\Psi$  in terms

of a cosine basis,  $\Psi(\mathbf{x}) = \sum_n c_n \cos(\frac{2\pi n x}{\Lambda})$ , with the finite number of coefficients  $\{c_n\}$  functioning as minimization parameters. As we show below, this choice not only offers a high degree of convergence, requiring typically less than a dozen coefficients, but also automatically satisfies the incompressibility or volume-conservation condition  $\int \Psi = 0$ , which would otherwise require an additional, nonlinear constraint. Note that the optimality and efficiency of the minimization can be significantly improved when local derivative information (with respect to the minimization parameters) is available, but given that even a single evaluation of  $\mathcal{E}_{\text{vdW}}[\Psi]$  is expensive—a tour-de-force calculation involving hundreds of scattering calculations [5]—this is currently prohibitive in the absence of an adjoint formulation (a topic of future work) [40]. Given our interest in equilibrium fluid shapes close to the initial condition of a flat fluid surface ( $\Psi = 0$ ) and because of the small number of degrees of freedom  $\{c_n\}$  needed to resolve the shapes, we find that local, derivative-free optimization is sufficiently effective, yielding fast-converging solutions.

In what follows, we compare the solutions of (3) based on (2) against those obtained through PFA and PWS, which approximate  $\mathcal{E}_{\text{vdW}}$  in this periodic geometry as:

$$\mathcal{E}_{\text{PFA}} = -\frac{\pi^2 \hbar c}{720} \int_{-\Lambda/2}^{\Lambda/2} dx \left( \frac{1}{h(x) - \Psi(x)} \right)^3 \quad (4)$$

$$\mathcal{E}_{\text{PWS}} = A \int_{-\Lambda/2}^{\Lambda/2} dx' \int_{-\infty}^{\infty} dx \int_{h(x')}^{\infty} dy' \int_{-\infty}^{\Psi(x)} dy \frac{1}{s^6}, \quad (5)$$

where  $A = -\frac{2\pi\hbar c}{45}$  is a Hamaker-like coefficient obtained by requiring that (5) yield the correct vdW energy for two parallel PEC plates, as is typically done [28]. Equation 5 is obtained from pairwise integration of the  $r^{-7}$  Casimir-Polder interactions following integration over  $z$  and  $z'$ , with  $r = \sqrt{s^2 + (z - z')^2}$  and  $s = \sqrt{(x - x')^2 + (y - y')^2}$  [41]. Note that because we only consider perfect conductors, there is no dispersion to set a characteristic length scale and hence all results can be quoted in terms of an arbitrary length scale, which we choose to be  $\Lambda$ . Additionally, we express the surface tension  $\gamma$  in units of  $\gamma_{\text{vdW}} = \frac{\pi^2 \hbar c}{720 d^3}$ , the vdW energy per unit area between two flat PEC plates separated by distance  $d$ . In what follows, we consider the impact of non-additivity on the fluid shape under both repulsive [Fig. 2] or attractive [Fig. 3] vdW pressures (obtained by appropriate choice of its sign), under the simplifying assumption of PEC surfaces interacting through vacuum. In either case, we consider local optimizations with small initial trust radii around  $\Psi = 0$ , and characterize the equilibrium fluid profile  $\Psi(x)$  as  $\gamma$  is varied. Our minimization approach is also validated against numerical solution of (1) under PFA (green circles).

**Repulsion.**— We first consider the effects of vdW repulsion on the equilibrium profile of the fluid–vacuum interface, enforced in our PEC model by flipping the sign of the otherwise attractive vdW energy. Such a situation can arise when a fluid film either sits on or is brought in close proximity to a solid grating [Fig. 2(insets)], causing the fluid to either wet or dewet

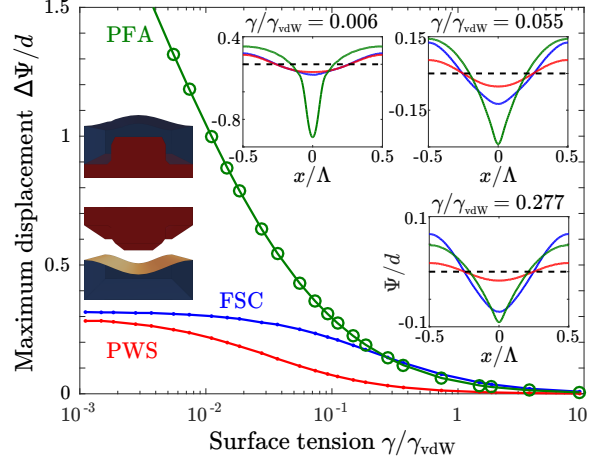


Figure 2. Maximum displacement  $\Delta\Psi/d$  of a fluid–vacuum interface that is repelled from a grating (insets) by a repulsive vdW force, as a function of surface tension  $\gamma/\gamma_{\text{vdW}}$ , obtained via solution of (3) using FSC (blue), PWS (red), and PFA (green) methods. Circles indicate results obtained through (1). Insets show the equilibrium fluid–surface profiles at selected  $\gamma \in \{0.006, 0.055, 0.277\}\gamma_{\text{vdW}}$ , with the unperturbed  $\Psi = 0$  surface denoted by black dashed lines.

the grating [6], respectively. Figure 2 compares the dependence of the maximum displacement  $\Delta\Psi = \Psi_{\text{max}} - \Psi_{\text{min}}$  of the fluid surface on  $\gamma$ , as computed by FSC (blue), PWS (red), and PFA (green). Also shown are selected surface profiles at small, intermediate, and large  $\gamma/\gamma_{\text{vdW}}$ . Note that the combination of a repulsive vdW force, surface tension, and incompressibility leads to a *local* equilibrium shape that is corroborated via linear stability analysis [42].

Under large  $\gamma$ , the surface energy dominates and thus all three methods result in nearly-flat profiles, with  $|\Psi| \ll d$ . While both additive approximations reproduce the exact energy of the plane–plane geometry (with the unnormalized PWS energy underestimating the exact energy by 20% [11]), we find that (at least for this particular grating geometry)  $\mathcal{E}_{\text{PWS,PFA}}/\mathcal{E}_{\text{FSC}} \approx 0.25$  in the limit  $\gamma \rightarrow \infty$ , revealing that even for a flat fluid surface, the grating structure contributes significant non-additivity. Noticeably, at large but finite  $\gamma \gg \gamma_{\text{vdW}}$ ,  $\Delta\Psi$  is significantly larger under FSC and PFA than under PWS, with  $\Psi_{\text{FSC,PWS}}$  exhibiting increasingly better qualitative and quantitative agreement compared to the sharply peaked  $\Psi_{\text{PFA}}$  as  $\gamma$  decreases [Fig. 2(insets)]. The stark deviation of PFA from FSC and PWS in the vdW-dominated regime  $\gamma \ll \gamma_{\text{vdW}}$  is surprising in that PWS involves volumetric interactions within the objects, whereas PFA and FSC depend only on surface topologies. Essentially, the pointwise nature of PFA means  $\mathcal{E}_{\text{PFA}}$  depends only on the local surface–surface separation, decreasing monotonically with decreasing separations and competing with surface tension and incompressibility to yield a surface profile that nearly replicates the shape of the grating in the limit  $\gamma \rightarrow 0$ . Quantitatively, PFA leads to larger  $\Delta\Psi$  as  $\gamma \rightarrow 0$ , asymp-



toting to a constant  $\lim_{\gamma \rightarrow 0} \Delta\Psi_{\text{PFA}} \rightarrow H = 3d$  at significantly lower  $\frac{\gamma}{\gamma_{\text{vdW}}} < 10^{-5}$ . On the other hand, both  $\mathcal{E}_{\text{FSC}}$  and  $\mathcal{E}_{\text{PWS}}$  exhibit much weaker dependences on the fluid shape at low  $\gamma$ , with the former depending slightly more strongly on the surface amplitude and hence leading to asymptotically larger  $\Delta\Psi$  as  $\gamma \rightarrow 0$ ; in this geometry, we find that  $\Delta\Psi_{\text{FSC,PWS}} \rightarrow \{0.32, 0.28\}d$  for  $\frac{\gamma}{\gamma_{\text{vdW}}} \lesssim 10^{-2}$ . Furthermore, while PFA and PWS are found to agree with FSC at large and small  $\gamma$ , respectively, neither approximation accurately predicts the surface profile in the intermediate regime  $\gamma \sim \gamma_{\text{vdW}}$ , where neither vdW nor surface energies dominate. Ultimately, neither of these approximations is capable of predicting the fluid shape over the entire range of  $\gamma$ .

*Attraction.*— We now consider the effects of vdW attraction, which can cause a fluid film either sitting on or brought into close proximity to a solid grating [Fig. 3(insets)] to dewet or wet the grating, respectively [6]. Here, matters are complicated by the fact that  $\mathcal{E}_{\text{vdW}} \rightarrow -\infty$  as the fluid surface approaches the grating, leading to a fluid instability or wetting transition below some critical  $\gamma^{(c)}$ , depending on the competition between the restoring surface tension and attractive vdW pressure. Such instabilities have been studied in microfluidic systems through both additive approximations [2, 4, 18, 43], but as we show in Fig. 3, non-additivity can lead to dramatic quantitative discrepancies in the predictions obtained from each method of computing  $\mathcal{E}_{\text{vdW}}$ . To obtain  $\gamma^{(c)}$  along with the shape of the fluid surface for  $\gamma > \gamma^{(c)}$ , we seek the nearest local solution of (3) starting from  $\Psi = 0$ . Figure 3 quantifies the onset of the wetting transition by showing the variation of the minimum grating-fluid separation  $h_{\min} - \Psi_{\max}$  with respect to  $\gamma$ , as computed by FSC (blue), PWS (red), and PFA (green), along with the corresponding  $\mathcal{E}_{\text{vdW}}$  [Fig. 3(inset)] normalized to their respective values for the plane-grating geometry (attained in the limit  $\gamma \rightarrow \infty$ ). Also shown in the top-right inset are the optimal surface profiles at  $\gamma \approx \gamma^{(c)}$  obtained from the three methods.

In contrast to the case of repulsion, here the fluid surface approaches rather than moves away from the grating, which ends up changing the scaling of  $\mathcal{E}_{\text{vdW}}$  with  $\Psi$  and leads to very different qualitative results. In particular, we find that  $\mathcal{E}_{\text{FSC}}$  exhibits a much stronger dependence on  $\Psi_{\max}$  compared to PWS and PFA, leading to a much larger  $\gamma^{(c)}$  and a correspondingly broad surface profile. As before, the strong dependence of  $\mathcal{E}_{\text{PFA}}$  on the fluid surface, a consequence of the pointwise nature of the approximation, produces a sharply peaked surface profile, while the very weak dependence of  $\mathcal{E}_{\text{PWS}}$  on the fluid shape ensures both a gross underestimation of  $\gamma^{(c)}$  along with a broader surface profile. Interestingly, we find that  $\gamma_{\text{FSC,PFA,PWS}}^{(c)} \approx \{0.65, 0.38, 0.07\}\gamma_{\text{vdW}}$ , emphasizing the failure of PWS to capture the critical surface tension by nearly an order of magnitude.

*Concluding Remarks.*— The predictions and approach described above offer evidence of the need for exact vdW calculations for the accurate determination of the wetting and dewetting behavior of fluids on or near structured surfaces. While we chose to employ a simple materials-agnostic and

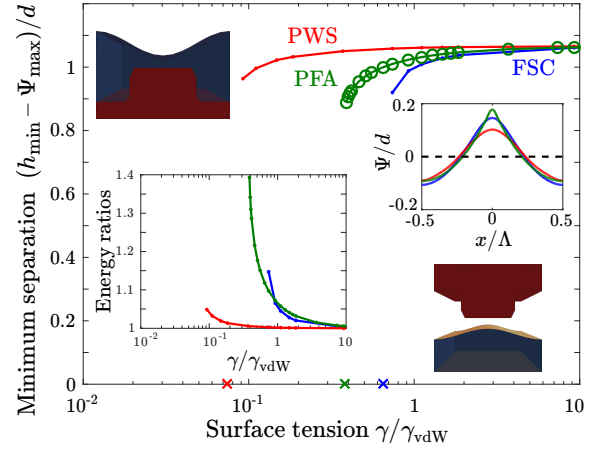


Figure 3. Minimum surface-surface separation  $\frac{h_{\min} - \Psi_{\max}}{d}$  of a fluid-vacuum interface that is attracted to a grating (insets) by an attractive vdW force, as a function of surface tension  $\frac{\gamma}{\gamma_{\text{vdW}}}$ , obtained via solution of (3) using FSC (blue), PWS (red), and PFA (green) methods. Circles indicate results obtained through (1). Wetting transitions occurring at critical values of surface tension  $\gamma^{(c)}$ , marked as 'x'. The top-right inset shows the equilibrium fluid-surface profiles near  $\gamma^{(c)}$  while the bottom-left inset shows the equilibrium vdW energies normalized by the energies of the unperturbed ( $\Psi = 0$ ) plane-grating geometry (the limit of  $\gamma \rightarrow \infty$ ).

scale-invariant model for the vdW energy, realistic (dispersive) materials can be readily analyzed within the same formalism, requiring no modifications. We expect that in these cases, non-additivity will play an even larger role. In fact, recent works [11, 16] have shown that additive approximations applied to even simpler structures can contribute larger discrepancies in dielectric as opposed to PEC bodies. For the geometry considered above, assuming  $\Lambda = 50$  nm and a nonretarded Hamaker constant  $A = 10^{-19}$  J [6, 28, 44], corresponding to a gold-water-oil material combination (with the thin  $d = 20$  nm water film taking the role of vacuum in our model), we estimate that significant fluid displacements  $\Delta\Psi \sim 10$  nm and non-additivity can arise at  $\gamma \approx 10^{-6}$  J/m<sup>2</sup>. By exploiting surfactants, it should be possible to explore a wide range of  $\gamma \in [10^{-7}, 10^{-2}]$  J/m<sup>2</sup> [18] and hence fluid behaviors, from vdW- to surface-energy dominated regimes. Yet another tantalizing possibility is that of observing these kinds of non-additive interactions in extensions of the original liquid He<sup>4</sup> wetting experiments that motivated development of more general theories of vdW forces (Lifshitz theory) in the first place [27]. In the future, it might also be interesting to consider the impact of other forces, including but not limited to gravity as well as finite-temperature thermodynamic effects arising in the presence of gases in contact with fluid surfaces.

*Acknowledgments.*— We are grateful to Howard A. Stone, M. T. Homer Reid, and Steven G. Johnson for useful discussions. This material is based upon work supported by the National Science Foundation under Grant No. DMR-1454836 and by the National Science Foundation Graduate Research Fellowship Program under Grant No. DGE 1148900.

- 
- [1] S. Prakash, M. Pinti, and B. Bhushan, *Philosophical Transactions of the Royal Society of London A: Mathematical, Physical and Engineering Sciences* **370**, 2269 (2012).
- [2] M. Geoghegan and G. Krausch, *Progress in Polymer Science* **28**, 261 (2003).
- [3] S. Chakraborty, “Microfluidics and microfabrication,” (Springer US, 2010) Chap. 3, pp. 113–130.
- [4] D. Bonn, J. Eggers, J. Indekeu, J. Meunier, and E. Rolley, *Reviews of Modern Physics* **81**, 739 (2009).
- [5] arXiv preprint.
- [6] J. N. Israelachvili, *Intermolecular and Surface Forces (Third Edition)*, third edition ed. (Academic Press, San Diego, 2011).
- [7] V. A. Parsegian, *Van der Waals Forces* (Cambridge University Press, 2005).
- [8] B. Derjaguin, *Kolloid-Zeitschrift* **69**, 155 (1934).
- [9] H. Hamaker, *Physica* **4**, 1058 (1937).
- [10] R. Büscher and T. Emig, *Phys. Rev. A* **69**, 062101 (2004).
- [11] A.-F. Bitbol, A. Canaguier-Durand, A. Lambrecht, and S. Reynaud, *Phys. Rev. B* **87**, 045413 (2013).
- [12] T. Emig, A. Hanke, R. Golestanian, and M. Kardar, *Phys. Rev. Lett.* **87**, 260402 (2001).
- [13] M. T. H. Reid, J. White, and S. G. Johnson, *Phys. Rev. A* **88**, 022514 (2013).
- [14] M. T. H. Reid, A. W. Rodriguez, J. White, and S. G. Johnson, *Phys. Rev. Lett.* **103**, 040401 (2009).
- [15] A. W. Rodriguez, P.-C. Hui, D. P. Woolf, S. G. Johnson, M. Lončar, and F. Capasso, *Annalen der Physik* **527**, 45 (2015).
- [16] C. Noguez and C. E. Román-Velázquez, *Phys. Rev. B* **70**, 195412 (2004).
- [17] J. C. Berg, “An introduction to interfaces & colloids: The bridge to nanoscience,” (World Scientific, 2010) Chap. 2, pp. 23–106.
- [18] D. B. Quinn, J. Feng, and H. A. Stone, *Langmuir* **29**, 1427 (2013).
- [19] R. Ledesma-Alonso, D. Legendre, and P. Tordjeman, *Phys. Rev. Lett.* **108**, 106104 (2012).
- [20] R. Ledesma-Alonso, P. Tordjeman, and D. Legendre, *Phys. Rev. E* **85**, 061602 (2012).
- [21] J. B. Sweeney, T. Davis, and L. E. Scriven, *Langmuir* **9**, 1551 (1993).
- [22] C. Bauer and S. Dietrich, *Phys. Rev. E* **60**, 6919 (1999).
- [23] A. Checco, O. Gang, and B. M. Ocko, *Phys. Rev. Lett.* **96**, 056104 (2006).
- [24] B. V. Derjaguin, I. I. Abrikosova, and E. M. Lifshitz, *Q. Rev. Chem. Soc.* **10**, 295 (1956).
- [25] H. B. G. Casimir and D. Polder, *Physical Review* **73**, 360 (1948).
- [26] A. D. McLachlan, *Proceedings of the Royal Society of London A: Mathematical, Physical and Engineering Sciences* **271**, 387 (1963).
- [27] I. E. Dzyaloshinskii, E. M. Lifshitz, and L. P. Pitaevskii, *Advances in Physics* **10**, 165 (1961).
- [28] L. Bergström, *Advances in Colloid and Interface Science* **70**, 125 (1997).
- [29] A. Rodriguez, M. Ibanescu, D. Iannuzzi, F. Capasso, J. D. Joannopoulos, and S. G. Johnson, *Phys. Rev. Lett.* **99**, 080401 (2007).
- [30] M. Bordag, *Phys. Rev. D* **73**, 125018 (2006).
- [31] A. Lambrecht, P. A. M. Neto, and S. Reynaud, *New Journal of Physics* **8**, 243 (2006).
- [32] S. K. Lamoreaux, *Phys. Today*.
- [33] M. T. Homer Reid and S. G. Johnson, *ArXiv e-prints* (2013), arXiv:1307.2966 [physics.comp-ph].
- [34] <http://homerreid.com/scuff-EM>.
- [35] E. Bormashenko, *Langmuir* **25**, 10451 (2009).
- [36] D. Silin and G. Vrnovsky, *Transport in Porous Media* **82**, 485 (2009).
- [37] Steven G. Johnson, The NLOpt nonlinear-optimization package, <http://ab-initio.mit.edu/nlopt>.
- [38] M. J. D. Powell, “A direct search optimization method that models the objective and constraint functions by linear interpolation,” in *Advances in Optimization and Numerical Analysis*, eds. S. Gomez and J.-P. Hennart (Kluwer Academic: Dordrecht, 1994), p. 51-67.
- [39] M. J. D. Powell, “The BOBYQA algorithm for bound constrained optimization without derivatives,” Department of Applied Mathematics and Theoretical Physics, Cambridge England, technical report NA2009/06 (2009).
- [40] M. B. Giles and N. A. Pierce, *Flow, Turbulence and Combustion* **65**, 393 (2000).
- [41] Note that in situations involving a deformed PEC surface and flat PEC plate, one can show that  $\mathcal{E}_{\text{PWS}} = \mathcal{E}_{\text{PFA}}$  [45], as this is a direct consequence of the additivity of the interaction.
- [42] I. Ivanov, “Thin liquid films,” (Taylor & Francis, 1988) Chap. 8.
- [43] T. Kerle, R. Yerushalmi-Rozen, J. Klein, and L. J. Fetters, *Europhys. Lett.* **44**, 484 (1998).
- [44] Y. Gu, *Journal of Adhesion Science and Technology* **15**, 1263 (2001).
- [45] T. Emig, A. Hanke, R. Golestanian, and M. Kardar, *Phys. Rev. A* **67**, 022114 (2003).